

Machine learning emulation of precipitation from km-scale regional climate simulations using a diffusion model

Henry Addison^{1,*}, Elizabeth J. Kendon^{2,1}, Suman Ravuri, Laurence Aitchison¹,
and Peter A.G. Watson¹

¹University of Bristol, Bristol, UK

²Met Office Hadley Centre, Exeter, UK

*Corresponding author: henry.addison@bristol.ac.uk

22nd July 2024

Abstract

High-resolution climate simulations are very valuable for understanding climate change impacts and planning adaptation measures. This has motivated use of regional climate models at sufficiently fine resolution to capture important small-scale atmospheric processes, such as convective storms. However, these regional models have very high computational costs, limiting their applicability. We present CPMGEM, a novel application of a generative machine learning model, a diffusion model, to skilfully emulate precipitation simulations from such a high-resolution model over England and Wales at much lower cost. This emulator enables stochastic generation of high-resolution (8.8km), daily-mean precipitation samples conditioned on coarse-resolution (60km) weather states from a global climate model. The output is fine enough for use in applications such as flood inundation modelling. The emulator produces precipitation predictions with realistic intensities and spatial structures and captures most of the 21st century climate change signal. We show evidence that the emulator has skill for extreme events up to and including 1-in-100 year intensities. Potential applications include producing high-resolution precipitation predictions for large-ensemble climate simulations and downscaling different climate models and climate change scenarios to better sample uncertainty in climate changes at local-scale.

1 Introduction

Understanding precipitation at a local scale is highly important for planning better climate change adaptation measures. Key challenges include representing the fine-scale structure of precipitation and effects such as convection. Convection is a key driver of many extreme events, but occurs at scales far below the typical resolutions of global climate models (GCMs) (Kendon et al. 2012). This has motivated using regional climate model (RCM) simulations at resolutions high enough to capture these processes, with GCMs providing boundary conditions (e.g. Kendon et al. 2021). These are known as regional convection-permitting models (CPMs). However, running a CPM is very computationally expensive, limiting sampling of climate change scenarios and extreme precipitation events. Furthermore, it is highly technically challenging to run a CPM with output from different GCMs (Sobolowski et al. 2023), limiting exploration of uncertainty in future climate projections at a local scale. Overcoming these challenges would allow for a much more comprehensive understanding of the range of potential severity of future extreme precipitation, for example through studying extreme events with large-ensemble GCM simulations (e.g. Maher et al. 2021; Leach et al. 2022) and to cover the range of climate change projections across different GCMs and emissions scenarios (e.g. Eyring et al. 2016).

Here, we demonstrate that a machine learning (ML) emulator of a CPM can produce realistic, high-resolution (8.8km) daily-mean precipitation simulations for England and Wales, conditioned

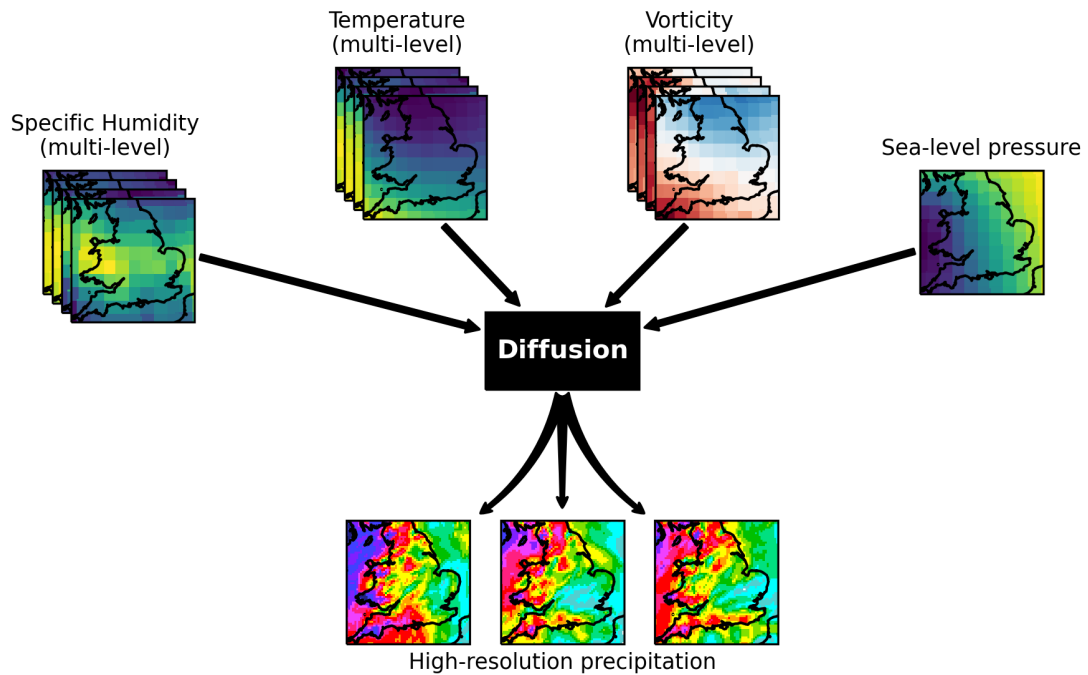


Figure 1: Schematic diagram of the inputs and outputs of the emulator. The emulator is trained to stochastically generate samples of high-resolution, daily mean precipitation over England and Wales (bottom panels). The target is for these samples to have properties matching output from the Met Office UK convection-permitting model. The emulator is stochastic, and can generate any number of samples for a single set of inputs. For input fields, the emulator takes variables at the same 60km resolution as the global climate model runs used to drive the CPM. These input fields are pressure at mean sea-level and specific humidity, temperature and vorticity at 250, 500, 700 and 850hPa (all daily means).

on GCM output. Our emulator is based on a diffusion model, a state-of-the-art generative ML approach (Sohl-Dickstein et al. 2015; Song et al. 2021). We call it “CPMGEM” (CPM Generative EMulator). A schematic diagram is shown in Figure 1. This produces samples at a small fraction of the computational cost of running a CPM at a resolution is fine enough to produce details of precipitation structures needed for applications such as flood modelling (e.g. Bates et al. 2023). We trained the emulator using output from the Met Office United Kingdom (UK) CPM, the first set of national-scale CPM climate simulations produced as part of the UK Climate Projections (UKCP) Local product (Kendon et al. 2021; Kendon et al. 2023).

There exists much previous work on developing statistical methods to predict high-resolution precipitation (e.g. Schoof 2013; Maraun and Widmann 2018). However, these methods have generally struggled to produce predictions with realistic spatial structure (Maraun et al. 2019; Widmann et al. 2019), which is important for predicting impacts such as flooding (e.g. Schaller et al. 2020; Archer et al. 2024). One particular challenge is representing the stochastic aspect of downscaling, where the coarse-scale weather state does not uniquely define the state at a finer scale (e.g. Maraun et al. 2017; Maraun et al. 2019). The stochastic component of precipitation at fine scales can have very complex structure, particularly when small-scale convection plays a substantial role. This is very difficult to represent with conventional statistical approaches.

The limitations of conventional statistics have motivated application of ML methods, which have been found to be able to make precipitation predictions with high-quality spatial structures. Some previous work has applied ML to downscale coarse-resolution precipitation predictions to capture high-resolution details (e.g. Vosper et al. 2023; Harris et al. 2022; Leinonen et al. 2020; Vandal et al. 2018; Sha et al. 2020). However, a CPM has potential to also improve the coarse-scale structure of precipitation events, particularly when convection plays a large role. Some studies have examined ML methods that do not use coarse-resolution precipitation as an input, learning to make predictions based on other fields that specify the weather state, potentially allowing learning of this large-scale added value. These have primarily focussed on deterministic approaches (e.g. Wang et al. 2023; Doury et al. 2024), but these fail to reproduce realistic, fine scale spatial structures compared to other work which use a stochastic component in modelling precipitation (e.g. Vosper et al. 2023; Ravuri et al. 2021; Harris et al. 2022; Hess et al. 2022). Recent work has also begun exploring the application of stochastic ML methods to predict precipitation based on non-precipitation predictor variables (Addison et al. 2022; Mardani et al. 2023), the approach we use here.

Whilst many statistical downscaling studies have focused on reproducing properties of observations (e.g. Gutiérrez et al. 2019), there is growing interest in learning to emulate high-resolution numerical models (e.g. Walton et al. 2015; Boé et al. 2022; Doury et al. 2023; Doury et al. 2024). The goal is to produce output similar to that of the numerical models at much reduced cost, enabling more complete sampling of climate change uncertainty and internal variability. One key advantage of learning to reproduce the output of high-resolution models is the ability to learn the effects of climate change from a physically-based model. For example, in the United Kingdom (UK), this includes complex effects such as summer rainfall becoming more concentrated into shorter, more intense downpours with climate change (Kendon et al. 2014; Kendon et al. 2021), which may be difficult to capture using a method trained on observations alone. Another advantage is having potentially larger datasets, which can help with learning a good representation of extreme events.

We show below that our emulator, which is stochastic, can predict samples of high-resolution precipitation with realistic spatial structures given coarse weather state information from a GCM, with climatological properties very close to those of the original simulations. A key challenge is representing extreme weather events, which may be anticipated to be especially difficult for ML approaches, and it is unclear how well they generally perform in this respect (Watson 2022; Watson 2023). We show evidence that our emulator represents events with intensities up to and including the ~ 1 -in-100 year return level well. We also show that the emulator captures most of the CPM’s climate change signal.

To our knowledge, our emulator is the first to be shown to satisfy a number of key requirements for high-resolution climate modelling together: producing output based on convective-scale simulations at a sufficiently fine resolution for impacts modelling, with realistic spatial structure,

and performing well at capturing structures and frequencies of extreme events with up to at least 100 year return periods, including when conditioned on GCM output data.

2 Results

We present results from our diffusion model-based emulator calculated from a test dataset of 108 simulated years that were not used in training. We first test the emulator using CPM data coarsened to the 60km GCM grid (cCPM) as input, to correspond to the inputs used in training. We use coarsened CPM for training to ensure alignment between coarse predictors and high-resolution precipitation structures. This is not always the case between the CPM and GCM variables, due to internal variability in the CPM (Doury et al. 2023). See Section 4 for more detail on the training process. Our next set of tests use predictors from the GCM to evaluate how well the emulator transfers to the challenge of predicting high-resolution precipitation when CPM data is not available, including capturing the climate change response. We use the terms “Diffusion-cCPM” to refer to our emulator using coarsened CPM inputs and “Diffusion-GCM” to refer to our emulator using GCM inputs. Finally, we evaluate the performance when there is a limited amount of training data.

2.1 Evaluation using coarsened CPM predictors

2.1.1 Evaluation on full domain

First, we evaluate our emulator using coarsened CPM data as inputs (“Diffusion-cCPM”), to test its performance in a similar situation to that used for training. We compare its predictions with those from a U-Net (“U-Net-cCPM”), a deterministic approach found to perform strongly in other studies on machine learning-based downscaling (Doury et al. 2023; Doury et al. 2024; Sha et al. 2020). We also compare with bilinear interpolation of the coarsened CPM precipitation (“cCPM Bilinear”). This is not a comparison downscaling method, as we do not use precipitation as a predictor in our emulator, but it is used to illustrate the effect of adding detail at length scales below the 60km grid spacing of the GCM.

We show example predictions of daily mean precipitation in Figure 2. This shows examples on days with substantial precipitation, selected according to the domain-mean value in the CPM. The first row is a wet day in winter, December–February (“DJF Wet”, the 80th percentile across domain means for all winter examples in the test subset). The second row is the wettest winter day (“DJF Wettest”, the winter example from the test set with the maximum domain-mean). The domain-mean precipitation in this example is only expected about once every 108 years, making this a test of the models’ skill for extreme events of intensities relevant to planning climate resilience (Watson 2022; Watson 2023). The third and fourth rows are similar but for summer, June–August (“JJA Wet” and “JJA Wettest”). Here, “JJA Wet” is an example chosen to have precipitation close to the 80th percentile and also a large region of convective showers, to illustrate the performance for this weather type. The other three examples show precipitation patterns characteristic of fronts.

The first column is the target CPM precipitation. The second column shows results from bilinear interpolation of coarsened CPM precipitation (cCPM Bilinear). The third column is vorticity at 850hPa derived from coarsened wind fields from the CPM. It is an example of the coarse inputs used by the emulator and provides a visualization of one of the features it sees.

The fourth and fifth columns show two samples from the diffusion model (randomly chosen from the six). These demonstrate the emulator’s ability to produce daily-mean precipitation samples with realistic fine detail. For DJF Wet it recreates the high intensity structures in the southern half of the domain whilst also having realistic lower intensity showers further north. For JJA Wet, it predicts small clusters of high intensity, similar to those seen in the CPM output. The predictions for the extreme examples in the second and fourth rows also correspond well to the CPM simulations. Note, since there is a substantial stochastic component of precipitation that is unpredictable given just the coarse-scale state, and selecting the most extreme day in CPM output will tend to select a day when this component is positive and relatively large, it

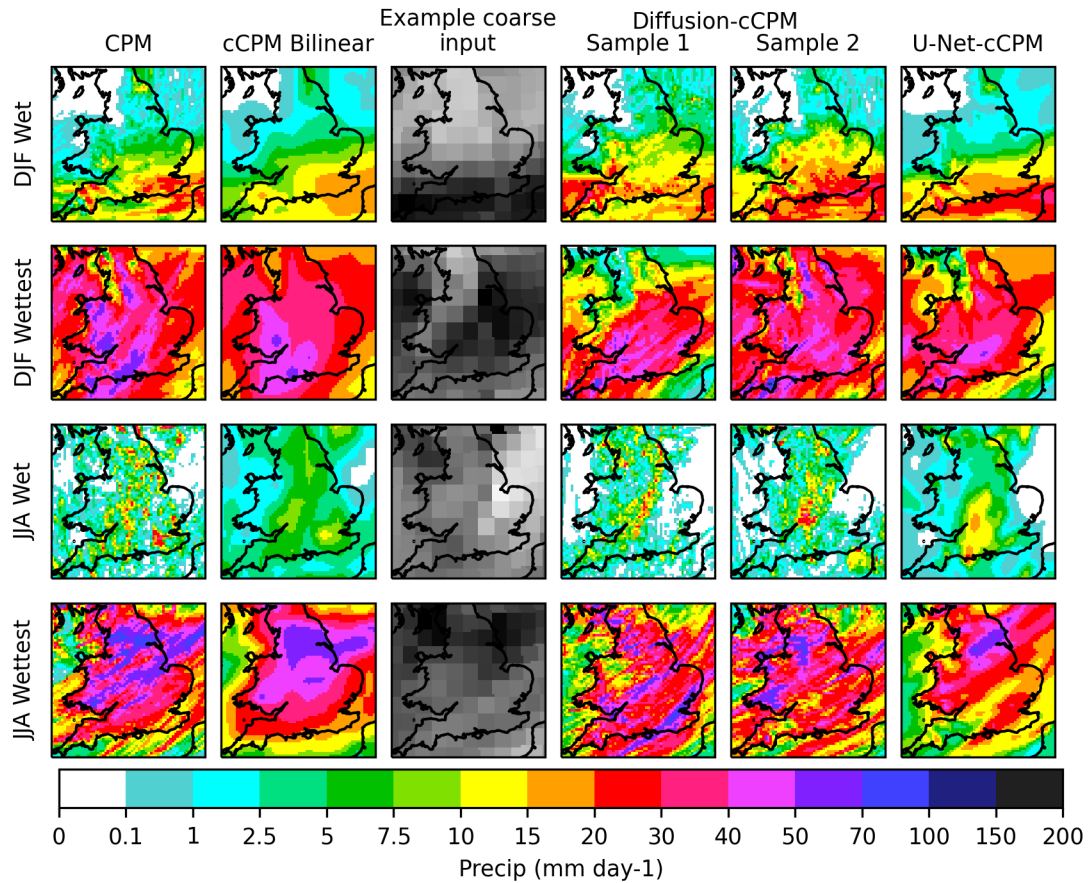


Figure 2: Examples of predictions of daily-mean precipitation. The first row is a wet day in winter (80th percentile of domain-mean). The second row is the wettest winter (December–February, DJF) day in the 108 year test dataset. The third and fourth rows are similar but for summer (June–August, JJA). The first column is the precipitation from the convection-permitting model (CPM). The second column is the coarsened CPM precipitation bilinearly interpolated to 8.8km resolution. Column 3 is an example coarse resolution input field, the 850hPa vorticity. Columns 4 and 5 are samples chosen at random from the emulator using coarsened CPM atmospheric variables as predictors (Diffusion-cCPM). Column 6 is the prediction by U-Net. Note that the highly stochastic nature of precipitation downscaling means samples from the diffusion model are not expected to match the CPM precipitation in full detail, but to represent the distribution of plausible precipitation fields for the given low resolution predictors, where the CPM simulation output is a single example.

Model	RMS Relative Mean Bias (%)	RMS Relative Std Dev Bias (%)
Diffusion-cCPM	3.4	3.6
Diffusion-GCM	2.7	4.6
U-Net-cCPM	14.2	19.9
cCPM Bilinear	10.4	13.8

Table 1: Root mean square of the relative biases. Computed across the 8.8km grid boxes for mean and standard deviation, as plotted in [Figure 3\(b,c\)](#).

would not necessarily be expected that typical samples from the emulator for the same day would reach as intense values as in the CPM.

The rightmost column shows predictions from the deterministic U-Net-cCPM. While it also mostly correctly represents the large-scale patterns (like the fronts in rows 2 and 4), it does not recreate the fine level detail of the CPM simulations, similar to other deterministic downscaling models (e.g. Doury et al. 2024; Sha et al. 2020). This is very noticeable in the JJA Wet case, for which it predicts a much smoother rainfall field, with lower peak intensity than seen in either the CPM or Diffusion-cCPM.

The differences between the two Diffusion-cCPM samples indicate the size of the stochastic component as learnt by the emulator. Whilst the large-scale features are fairly similar, as expected since the samples are conditioned on the same coarse-scale input, the locations of the heaviest precipitation amounts generally differ, which may result in very different local impacts. This indicates that the stochastic component is large and it is important that it is represented. The Diffusion-cCPM samples also illustrate how the emulator could generate different realisations of a given day’s precipitation, perhaps to explore the impact were the heaviest downpours to happen in different locations, for example in areas with critical infrastructure. (This could be an interesting application of a similar emulator trained on observations and applied to historical weather events, although we do not explore this here.)

As well as producing realistic samples, it is important that the frequency distribution of precipitation produced by the emulator matches that of the CPM. [Figure 3\(a\)](#) shows the frequency distribution of precipitation across all 8.8km grid boxes for the CPM, the downscaling models and the results of cCPM Bilinear. The distribution of Diffusion-cCPM matches that of the CPM distribution very closely up to intensities of over 200 mm/day, the extreme tail of the test set (there are only two CPM simulated values beyond the maximum shown). Note the log scale of the density axis.

Both U-Net-cCPM and cCPM Bilinear have too low frequencies of precipitation more intense than ~ 30 mm/day. Potentially for U-Net-cCPM, this could be improved by using a loss function designed to increase prediction of extreme values Doury et al. (e.g. 2024). However, it would also be expected that the stochastic aspect of Diffusion-cCPM contributes to generating an accurate frequency of extreme values.

Importantly, the Diffusion-cCPM emulator also predicts a similar frequency of wet days as the CPM. The frequency of days with more than 0.1mm of precipitation in individual 8.8km grid boxes is 52.6% for Diffusion-cCPM versus 53.0% for the CPM (66.4% versus 67.4% in winter and 36.9% for both cases in summer).

The precipitation distribution varies across the UK, due to effects such as elevation. [Figure 3\(b\)](#) and [\(c\)](#) show spatial maps of the biases in the mean and standard deviation. Diffusion-cCPM displays small biases over the whole domain. U-Net-cCPM has a consistent dry mean bias everywhere and a too low standard deviation (Doury et al. (2024) found similar), again indicating the likely role of the stochastic part of the precipitation variability in the diffusion model emulator. The cCPM Bilinear biases are substantial in areas with high terrain, such as northwest and southwest England and Wales, where there is high spatial variance. The comparison with Diffusion-cCPM shows that the emulator has learnt the differences in precipitation properties between nearby locations, below the scale of the coarse-resolution inputs. [Table 1](#) summarises the root mean squares of these biases over space, quantifying the typical sizes of these biases.

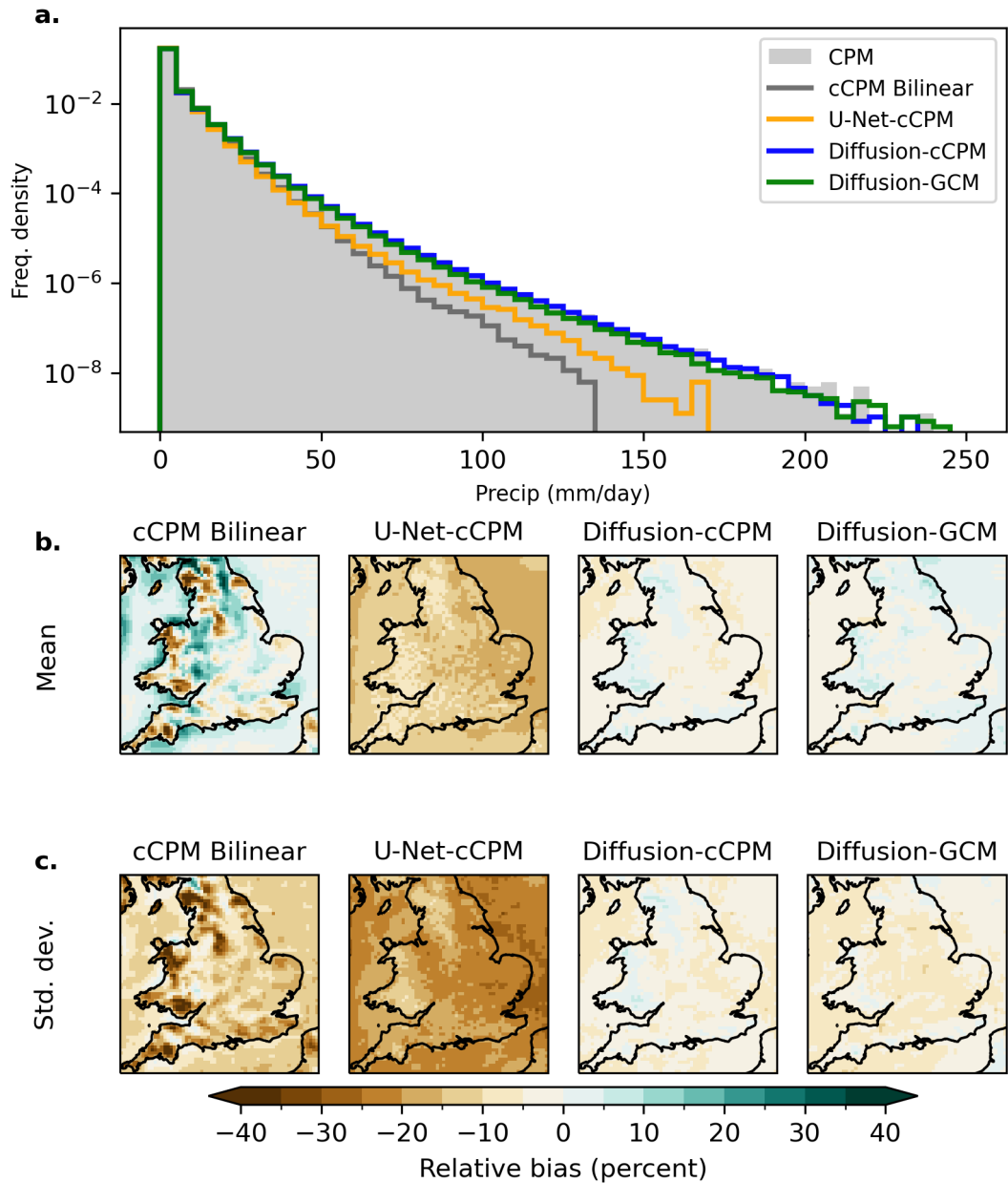


Figure 3: Distribution of predictions. (a) Histograms of precipitation values on the 8.8km grid. The grey shaded area is the frequency density of the target CPM precipitation. The lines show frequency densities from the diffusion model emulator acting on coarsened CPM and GCM inputs respectively (“Diffusion-cCPM” (blue) and “Diffusion-GCM” (green)), U-Net-cCPM (orange) and CPM precipitation coarsened to 60km resolution with bilinear interpolation (cCPM Bilinear; dark grey). Note the vertical axis is logarithmic. (b) Relative mean bias as a percentage of the CPM mean for each model. (c) Same as (b) but for standard deviation bias.

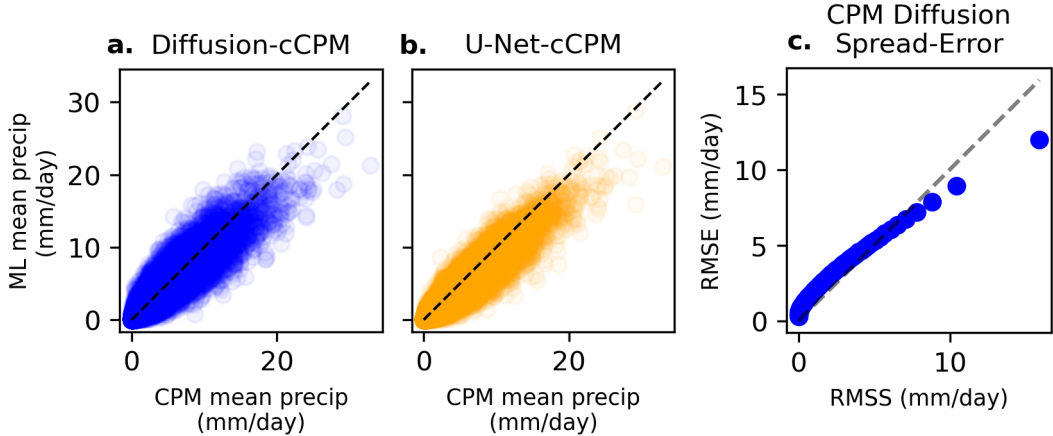


Figure 4: Spread of predictions. (a) Scatter plot of daily domain-mean precipitation for samples from Diffusion-cCPM versus target CPM values. (b) Same as (a) for U-Net-cCPM. (c) Spread-error plot of Diffusion-cCPM, indicating the calibration of the stochastic component (see main text for details).

As well as matching the climatological distribution of CPM precipitation, the emulator must also learn the dependence of the precipitation distribution on the coarse input variables. We examine this using a scatter plot of domain-mean precipitation from Diffusion-cCPM against that from the CPM target (Figure 4(a)). We use the domain-mean because this reduces the variability from the stochastic component sufficiently to be able to clearly see that the predicted and target precipitation are well-correlated. Note that since precipitation likely has a substantial stochastic component that is unpredictable given only coarse-scale variables, a perfect correlation could not be expected. The degree of correlation is similar for U-Net-cCPM (Figure 4(b)), though this shows some systematic underestimation. This indicates that the deterministic component of Diffusion-cCPM (identified conceptually with the mean over many samples) is similarly skilful to predictions from U-Net. Both appear to learn a skilful relationship between the inputs and total precipitation. The stochasticity in the Diffusion-cCPM output likely contributes to its predictions having slightly more spread.

It is also important to evaluate whether the size of the stochastic component of the Diffusion model emulator is appropriate. We follow the approach of Leutbecher and Palmer (2008) and produce a spread-error plot (Figure 4(c)), also discussed by Haynes et al. (2023). The idea is that if the CPM simulation output is statistically similar to samples from the emulator, as in the ideal case, then the relationship with the mean of the samples should be identical for CPM and emulator outputs. Then the root mean square difference between the emulator ensemble mean and the CPM output (the root mean square error, RMSE, of the ensemble mean) and the root mean square difference between the emulator ensemble mean and the individual emulator samples (the root mean square spread, RMSS) should be equal, given a correction factor depending on the number of predictions and ensemble size. This is also the case if samples are binned into intervals of the RMSS. The spread-error plot compares the RMSE and RMSS within these bins, with values calculated for every grid box and example in the test dataset.

Figure 4(c) shows the RMSE versus RMSS for Diffusion-cCPM. We compute the squared spread of emulator samples and squared error for the mean of the samples for each grid box in every example of the test subset. We group these pairs of spread and error into bins containing an equal number of values according to this spread and plot the RMSS and the corresponding RMSE for the predictions in each bin. As desired, Diffusion-cCPM does have approximately equal RMSE and RMSS across most of the range of spread values, indicating that the stochastic component of the predictions has an appropriate size, and that the model can skilfully differentiate between situations that are relatively predictable (low spread and error) and less predictable (high spread and error). There is a slight tendency for the emulator to be

overconfident for cases with lower spread and to be more noticeably underconfident for cases with higher spread.

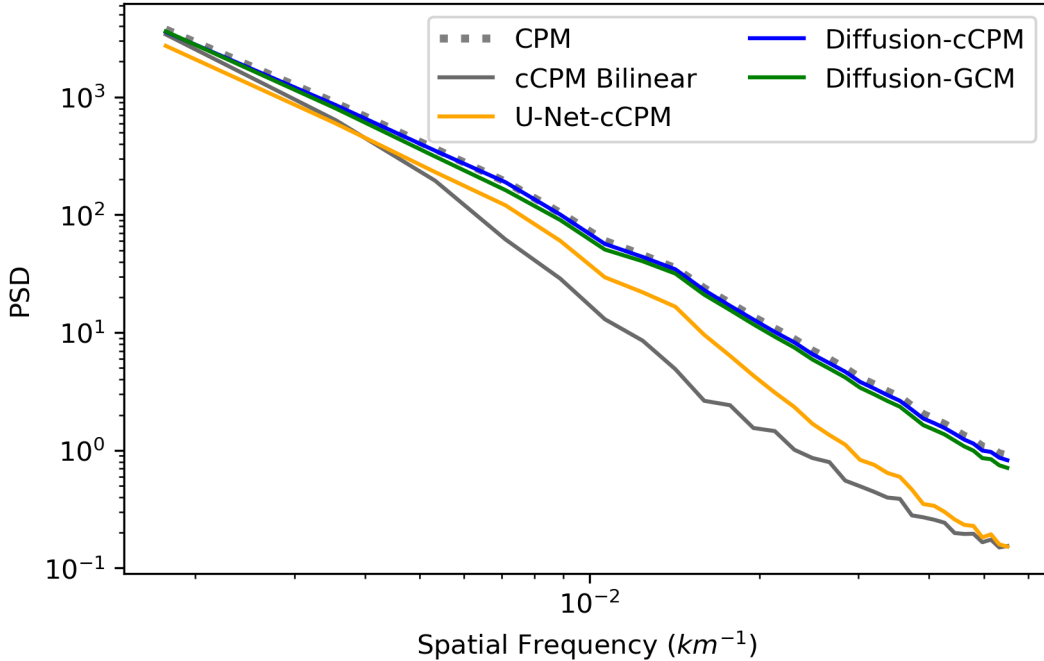


Figure 5: Radially averaged spatial power spectral density (RAPSD). Shows the target CPM precipitation (grey dashes), the emulator samples, Diffusion-cCPM (blue line) and Diffusion-GCM (green line), U-Net-cCPM (orange) and cCPM Bilinear (dark grey).

To quantitatively evaluate the realism of the spatial structures in the emulator output, we show the radially averaged power spectral density (RAPSD, see [Section 4.4](#) for more detail) in [Figure 5](#). This quantifies the amount of variance across the range of spatial scales in the data. The RAPSD of the CPM and Diffusion-cCPM match closely for the full frequency domain, showing that Diffusion-cCPM produces structures which have similar variability at different spatial scales to the CPM simulation. The close agreement at small spatial scales (high frequencies) reflects how the Diffusion-cCPM samples include a realistic degree of fine-scale structure, as seen in the samples in [Figure 2](#). The curves for U-Net and cCPM-Bilinear generally display too low variability, particularly at the highest frequencies, corresponding to these predictions having unrealistically smooth small-scale structure, though comparing with cCPM Bilinear indicates that U-Net does appear to add some variability below the scale of the coarse grid. Comparing the results for the diffusion model and U-Net indicates that including a stochastic component in the emulator samples has helped to realistically represent small-scale variability.

2.1.2 Regions, seasons and different precipitation types

Different processes drive UK precipitation to different extents depending on the region and time of year. Therefore we evaluate whether the emulator reproduces these differing regional and seasonal characteristics of precipitation. [Figure 6](#) shows frequency distributions for precipitation in northwest England in winter and in the southeast in summer across individual points on the high-resolution grid. In the former case, precipitation is predominantly frontal and orographic, while the latter case has a larger convective component. Both regions are 16×16 8.8km grid boxes in size.

The frequency distribution of Diffusion-cCPM samples closely follows that of CPM precipitation for both the northwest in winter and the southeast in summer. The same is not true of samples from U-Net-cCPM, which matches the northwest winter distribution well until about

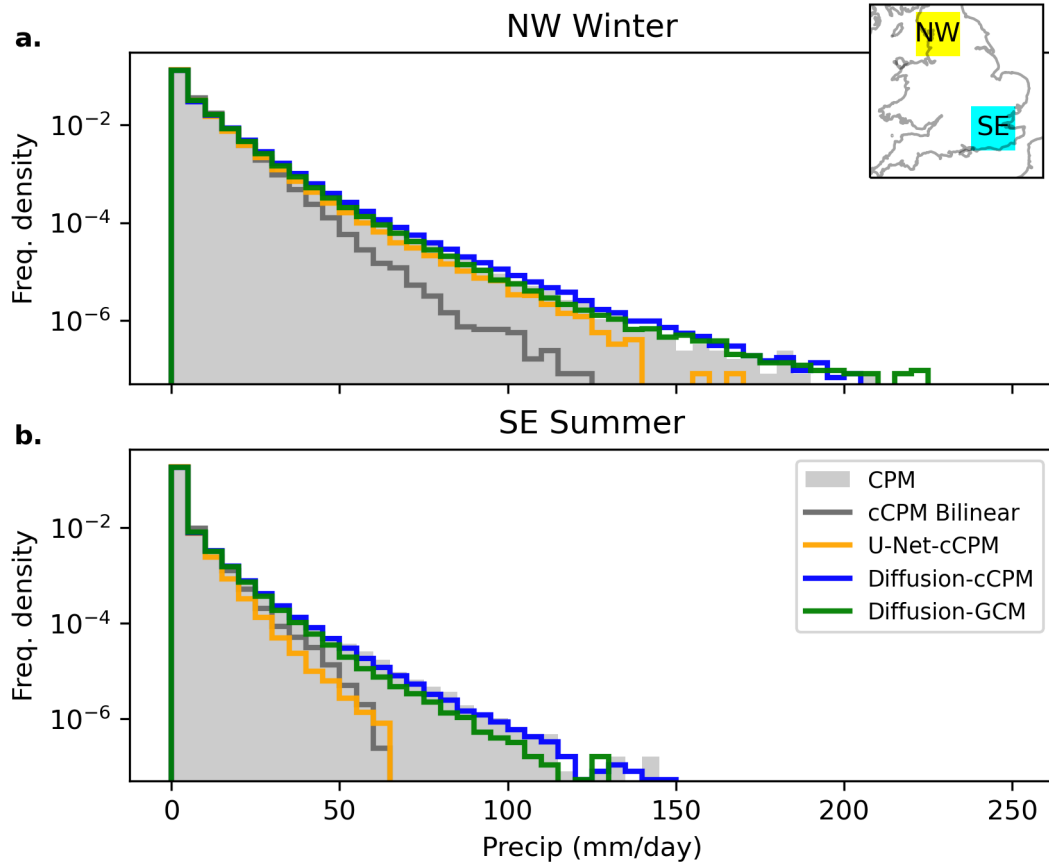


Figure 6: Comparisons for different regions and seasons. Frequency distributions of precipitation intensity in different seasons and regions: (a) winter in northwest England, where precipitation is predominantly frontal and orographic; (b) summer in southeast England, which includes a substantial convective precipitation component. Plotted as in Figure 3(a). The inset at the top right shows the regions in the context of the full spatial domain.

125mm/day, but substantially underpredicts the frequency of more extreme intensities, as for the full frequency distribution shown in Figure 3(a). The agreement between the target CPM and U-Net-cCPM is closer than for the full distribution, suggesting that the deterministic component of precipitation in this region and season accounts for a larger share of variability, perhaps due to the strong orographic component and importance of large-scale frontal systems, with the stochastic component being more apparent in the most intense extremes. cCPM Bilinear produces a large underestimate for frequencies greater than about 25mm/day, indicating the relevance of small-scale variability. In the southeast in summer, both U-Net-cCPM and cCPM Bilinear similarly underestimate the frequency of heavy precipitation. This indicates an important role for the stochastic component of precipitation here, which may be expected given the larger influence of small-scale convective rainfall systems than in the NW Winter case, as in the example in the third row in Figure 2.

2.2 Transfer to using GCM inputs

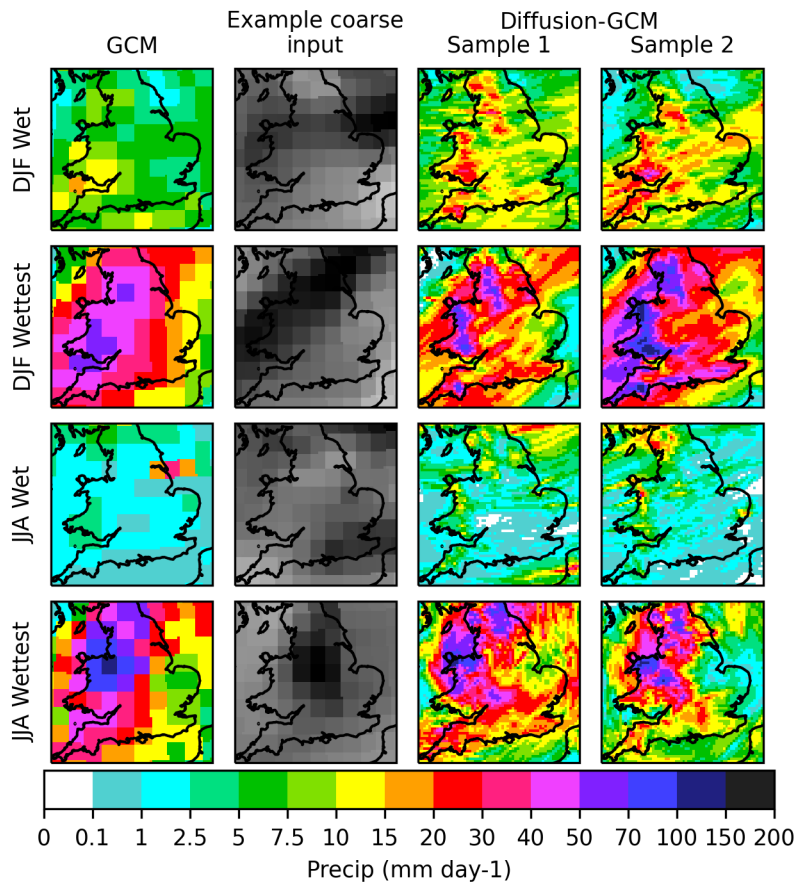


Figure 7: Samples based on GCM input variables. Each row shows results for one example day, chosen in a similar way to those in Figure 2, based on domain-mean GCM precipitation. The first column shows the GCM precipitation, the second an example coarse input field (vorticity at 850hPa) and columns 3 and 4 are two samples from the emulator using GCM inputs. Note the emulator output is not constrained to match the coarse-resolution structures of the GCM precipitation, and may predict more realistic features at large as well as small scales.

Next we examine how well our emulator transfers to the problem of downscaling GCM data, rather than the coarsened CPM data like that used for training. We focus just on the performance of the Diffusion-GCM emulator.

Figure 7 shows example predictions from the Diffusion-GCM model, which includes bias correction of the mean and variance of the predictors, learnt from the training dataset (see Section 4.3.3 for details). The rows each correspond to a different day and are chosen in a similar way as in Figure 2, but based on GCM precipitation, with “DJF Wet” and “JJA Wet” days corresponding to the 80th percentile of the domain-mean, and the other two rows to the wettest winter or summer day in the test subset respectively. The first two columns show data from the GCM for context: the low resolution precipitation and one input to the emulator, the coarsened vorticity at 850hPa. The third and fourth columns show two samples from Diffusion-GCM for the given predictor variables. It can be seen that they contain finer spatial detail. Also they do not in general have exactly the same coarse-scale spatial structure as the GCM simulation, as they have learnt a separate model of precipitation based on the CPM target, and so do more than just add spatial detail to the precipitation. For example, Diffusion-GCM predicts heavier precipitation in the western UK in the “DJF Wet” case and in the northern England in the “JJA Wet” case.

Figure 3(a) shows that when working on GCM-derived inputs the emulator (Diffusion-GCM) continues to produce samples whose distribution of intensities is still very similar to the CPM precipitation target on the 8.8km grid. It also predicts a similar proportion of wet days (with $>0.1\text{mm/day}$) to the CPM across all grid boxes: 53.0% annually from the emulator compared to 54.7% from the CPM. Seasonal differences in this proportion are also captured by the emulator: 67.4% compared to 68.1% in winter and 36.9% compared to 38.4% in summer. The biases in the mean and standard deviation of precipitation of Diffusion-GCM are small relative to the CPM target throughout the spatial domain (Figure 3(b) and (c) and Table 1) and the spatial power spectral density for Diffusion-GCM is very similar to Diffusion-cCPM and the CPM as well (Figure 5). For the NW winter and SE summer (Figure 6), the frequency distributions of precipitation are also very similar, albeit with a slight underestimation of the frequency of days with more than 50mm/day in SE Summer. This indicates that the emulator produces precipitation samples with realistic structure and intensities when given as input bias-corrected GCM variables. Without this adjustment, the emulator had a dry bias across the whole domain, discussed by (Kendon et al. 2024).

To indicate how much closer the emulated precipitation is to the CPM output than the GCM precipitation, Figure 8 compares statistics of precipitation on the GCM’s coarse grid between the GCM output and conservatively regridded Diffusion-GCM and CPM output. The emulator produces a similar distribution of intensities to the CPM at this coarser scale right up to around the maximum coarsened CPM value from the test set, about 120mm/day (panel (a)). The distribution of GCM precipitation, however, has an exaggerated tail for values larger than about 50 mm/day. The biases in the mean and standard deviation are much smaller for the emulator than for the GCM, particularly in grid boxes covering upland areas and near the western and southern coasts (Figure 8(b) and (c)).

2.3 Climate change comparison

As mentioned in the introduction, a key advantage of training on high-resolution simulation data is the potential ability to learn a physically-based climate change signal. Figure 9 shows the emulator’s ability to capture the effect of climate change on the precipitation frequency distribution, including extremes. Panel (a) shows the differences in the frequency distribution of precipitation from our emulator (Diffusion-GCM) for the three time periods (“Historic” for 1981–2000, “Present” for 2021–2040 and “Future” for 2061–2080). There is an increase in intensities in the tail of the emulator’s distribution as time increases. The other three panels compare distributions from Diffusion-GCM, the CPM target and the CPM in the Historic period, to show the realism of the emulator’s climate change signal. The emulator distributions closely match the CPM target for all three time periods, and the shift away from the Historic distribution over time as seen particularly clearly in the Future period.

As well as an overall change in annual distribution, there are seasonal and spatial dependencies in the differences. It is projected that the UK will become drier in the summer and wetter in the winter (Kendon et al. 2021). Figure 10 shows the relative change in the mean precipitation

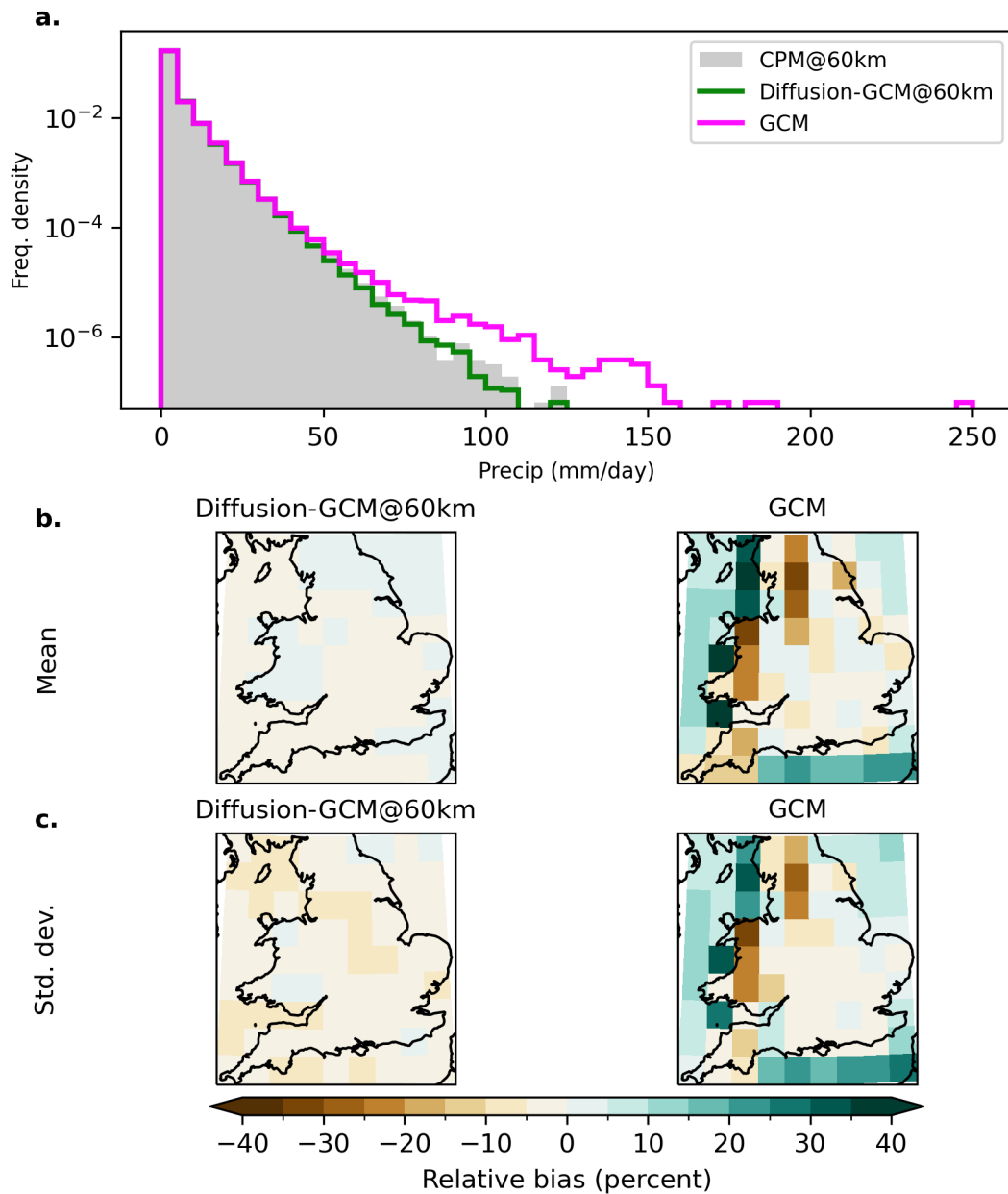


Figure 8: Comparison at GCM scale. (a) Histograms of daily precipitation values on the 60km grid, for the coarsened target CPM precipitation (grey filled area), the coarsened output of the Diffusion-GCM emulator (green), and GCM precipitation (magenta). Note the vertical axis is logarithmic. (b) Relative bias in mean precipitation compared to the CPM for Diffusion-GCM (left) and GCM (right) on the coarse grid (in contrast to results shown for precipitation on the fine grid in [Figure 3\(b\)](#)). (c) Same as (b) but for standard deviation bias.

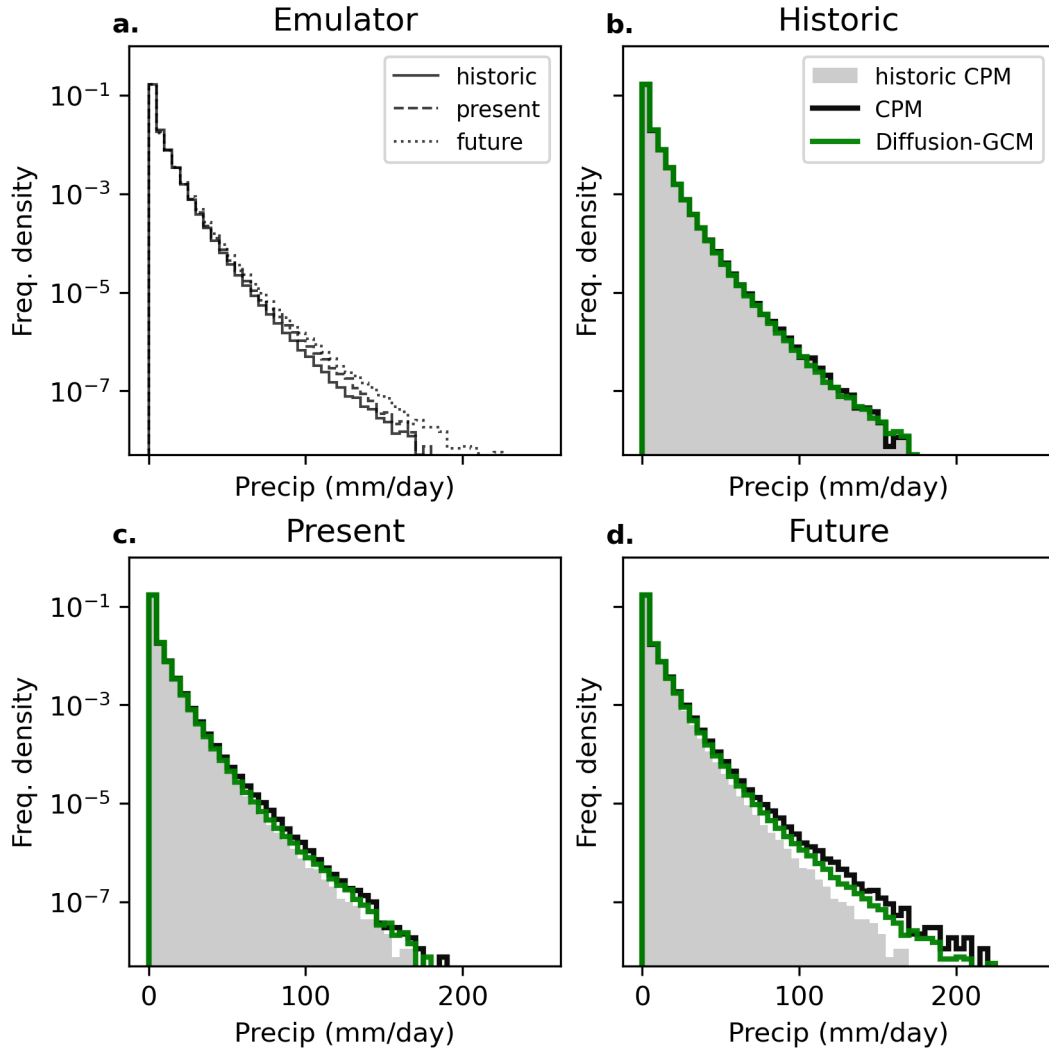


Figure 9: Climate change effect on precipitation frequency distributions. (a) shows the different Diffusion-GCM frequency densities for the three different time periods: Historic (solid black), Present (dashed black) and Future (dotted black). (b) shows a comparison of the frequency density histogram of Diffusion-GCM (green) with the CPM (black) for the Historic time period. (c) and (d) show the same as (b) but for Present and Future time periods respectively. In (b), (c) and (d) the filled grey histogram shows the CPM precipitation frequency distribution from the Historic time period to highlight the change in the precipitation distribution between the time periods.

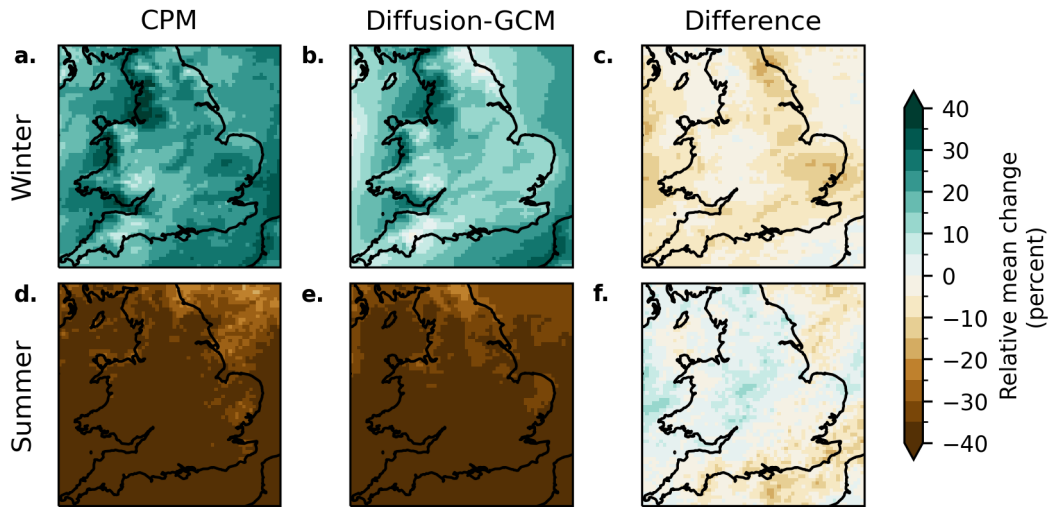


Figure 10: Changes in seasonal mean precipitation from 1981–2000 to 2061–2080. (a, b, c) show results for winter and (d, e, f) results for summer. The first column (a, d) is the relative change in the mean for the CPM, the second column (b, e) the same for the emulator, Diffusion-GCM. In both cases the changes are shown as percentages of the Historic CPM seasonal mean. The third column (c, f) is the difference between the Diffusion-GCM and CPM changes.

Season	CPM (%)	Diffusion-GCM (%)	Difference (95% CI) (% of CPM change)	Difference (95% CI) (% of Historic CPM)
Winter	23	17	-26 (-41 to -10)	-5.9 (-9.5 to -2.2)
Spring	6	2	-61 (-134 to +13)	-3.8 (-8.3 to +0.8)
Summer	-40	-39	2 (-18 to +14)	0.8 (-5.7 to +7.1)
Autumn	-4	-8	+114 (-13 to +240)	-4.5 (-9.4 to +0.5)

Table 2: Change in seasonal domain mean for Diffusion-GCM. Shows changes in the domain mean from Historic to Future periods for each season. The second and third columns contain the relative changes for the CPM and Diffusion-GCM respectively (relative to CPM Historic seasonal domain mean in both cases). The fourth column contains the difference between the change in the CPM and Diffusion-GCM, relative to the change in CPM. The values in brackets in these columns are the bootstrapped 95% confidence intervals of the difference. The fifth column is the same as the third but relative to the Historic CPM seasonal domain mean.

between Historic and Future time periods for winter (top row; a, b, c) and summer (bottom row; d, e, f) for both the CPM (left column; a, d) and Diffusion-GCM (middle column; b, e). The right column (c, f) shows the difference between the mean changes in the CPM and in the emulator.

The emulator reproduces the mean drying in summer well. Summer is a particularly important season for the emulator to represent well, as a large component of UK summer rainfall is convective, and the UK CPM predicts changes in rainfall intensities that are substantially larger than in climate models with lower resolutions (Kendon et al. 2017). The emulator also captures most of the wetting in winter, though there is some underestimation. Table 2 shows the change in seasonal domain means. The change in summer is reproduced very accurately, but the winter change is underestimated by 26% (95% confidence interval 10–41% from bootstrapping, see Section 4.5 for more details). The results indicate that the changes in spring (March–May, MAM) and autumn (September–November, SON) are also reproduced with the correct sign, but there is some evidence of underestimation and overestimation of the magnitude respectively. However, the magnitude of the mean changes in these seasons is relatively small, giving high sampling uncertainty of the relative differences, and their 95% confidence intervals overlap with zero. The values are similar for Diffusion-cCPM (see Table S3 in Supplementary Materials). A possible reason for there being some error in the prediction of the mean changes is that the climate change signal does not account for a large fraction of the variance of precipitation between randomly chosen days, so that the standard ML approach of optimising a skill score evaluated on each prediction independently does not provide adequate information to improve the mean change. Therefore it may be valuable to develop modified training procedures that place more weight on capturing the climate change signal, such as using different loss functions. Including additional predictor variables may also give better performance.

The emulator predicts similar changes of frequencies in wet days (again, $>0.1\text{mm/day}$) across all grid boxes: a 2% relative increase in wet days in winter (mean of changes at every grid box) versus a 5% increase in the CPM, and a 38% decrease in summer versus 36% in the CPM. The lower increase in winter wet days contributes to underestimation of the predicted mean precipitation increase.

2.4 Training with smaller datasets

We briefly discuss whether similar results could be obtained using CPM datasets of smaller size, $\sim 10\text{--}20$ years, corresponding to the amount of data available from some projects (e.g. Chan et al. 2020; Kendon et al. 2019), as opposed to the *sim*500 years that we used to train the emulator discussed above. This is important for considering how widely the method could be applied. We train the low-data emulator Diffusion_ld on a much smaller dataset (14 years, one ensemble member in the Historic time period, $\sim 3\%$ of the full training dataset size). We test it on the portion of the test dataset from the Historic time period and the same ensemble member as used for training (3 years). We find that, using either cCPM or GCM inputs, this emulator is able to recreate the frequency distribution of the CPM precipitation well (Figure 11(a)). Individual samples and the spatial power spectrum still appear realistic (Figure 11(b,c)). Therefore the method does seem able to produce output matching the climatological CPM properties with this amount of data. The main challenge may be verification. With low amounts of high-resolution model data, it would be difficult to evaluate an emulator’s performance on rare, high-impact weather events, although there are methods that may assist (Watson 2022). It would also be difficult to verify the emulated climate change signal, since there would be high sampling variability with such small amounts of data.

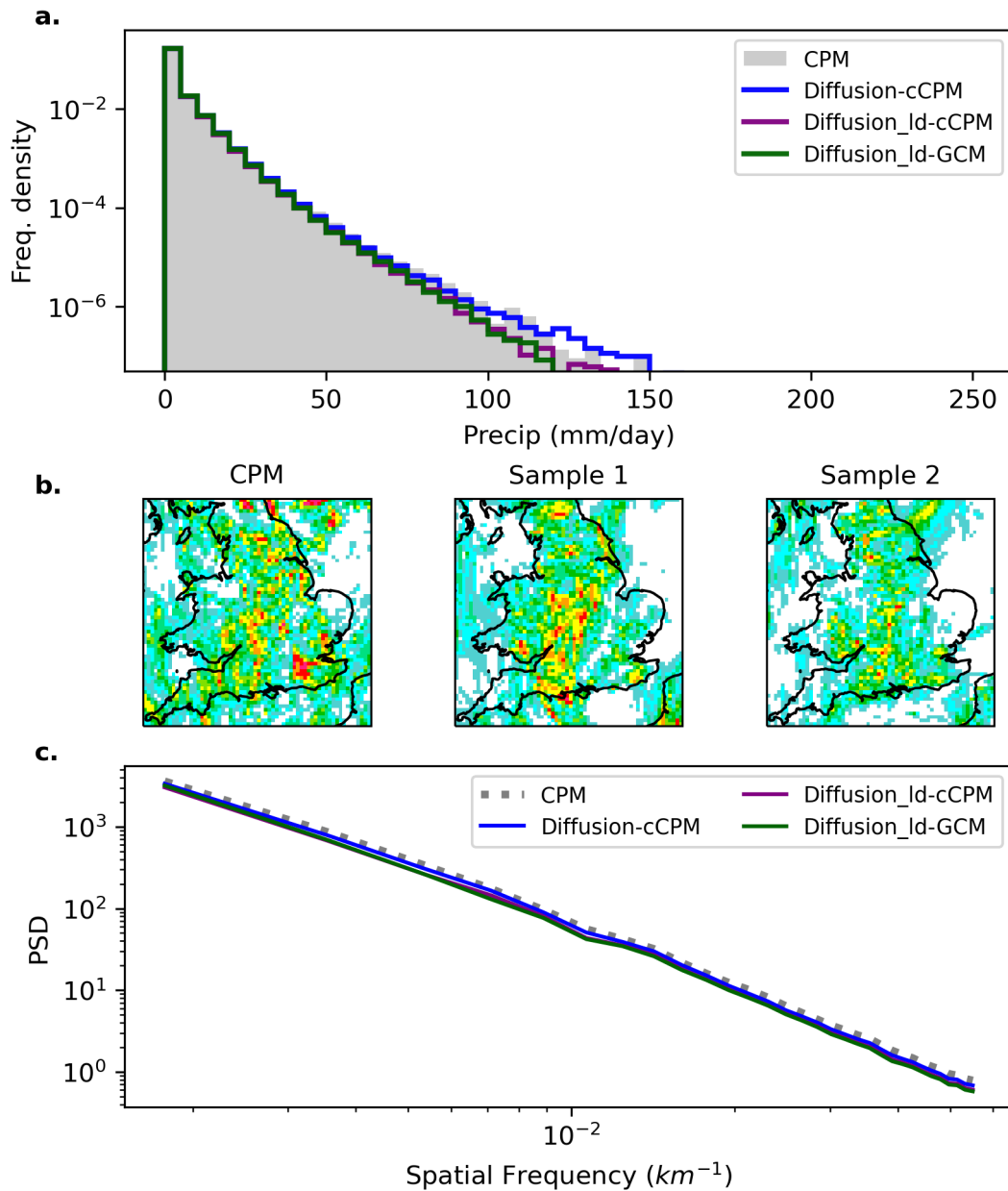


Figure 11: Results for an emulator developed using a reduced (fourteen year) training dataset. Both training and test data are from one ensemble member for the Historic time period only. (a) Histograms of precipitation values on the 8.8km grid: for the target CPM precipitation (grey filled area), the emulator developed using the full training data (Diffusion-cCPM, blue), and an emulator trained on the reduced data using coarsened CPM and GCM inputs: Diffusion_ld-cCPM (purple) and Diffusion_ld-GCM (dark green) respectively. Note the vertical axis is logarithmic. (b) Samples from the same "JJA Wet" day as in Figure 2, from the CPM (left) and two samples from Diffusion_ld-cCPM (middle and right). (c) Radially-averaged spatial power spectral density (PSD) for the target CPM precipitation (grey dashed) and each emulator (colours as (a)).

3 Discussion and conclusions

We have demonstrated an emulator of a regional CPM based on a diffusion model, a generative machine learning method. It is able to produce samples of high-resolution (8.8km), daily-mean precipitation with realistic properties, conditional on coarse-resolution (60km) variables from the Met Office GCM. It has a much lower computational cost than the CPM. The output is at high enough space and time resolution for applications such as flood inundation modelling (Bates et al. 2023) and we have shown evidence that the emulator produces predictions with realistic structure and frequency for extreme events with return times up to ~ 100 years. The 21st century climate change signal is captured well in summer, the season when the CPM’s representation of convective processes is most valuable, but there is evidence of some error in the mean change in other seasons. We have used a ~ 500 year training dataset for our main results, but also find that a good reproduction of climatological precipitation properties can also be obtained given only 14 years of training data.

The emulator is stochastic, and the stochastic component is reasonably well-calibrated, so that the emulator can create a range of plausible high-resolution samples for given large-scale conditions. From comparison to a deterministic U-Net model and other studies in the literature, the stochastic component is important for producing precipitation predictions with realistic small-scale structure and predicting the correct frequency of the most extreme intensities.

Routes for further development include increasing the output resolution and domain size in space and time yet further. Recently developed “video diffusion” methods (e.g. Blattmann et al. 2023; Bar-Tal et al. 2024; Harvey et al. 2022) could be applied to improve temporal coherence, likely to be important for producing sub-daily predictions. Generating multi-variate output is another key target for climate impacts modelling. Further directions for evaluating the emulator include testing it with output from other GCMs, critical for application to augment available CPM simulations, and assessing how realistic are the results if the emulator’s outputs are used to model impacts, such as flood inundation. Our results also indicate that improving ML methods so that they better capture the climate change signal would also be highly valuable.

4 Materials and methods

4.1 Data

CPM data for training and evaluation are taken from the UKCP Local product (Kendon et al. 2023; Kendon et al. 2021) and the GCM data is from UKCP18 Global simulations that were used to produce boundary conditions for the CPM (Murphy et al. 2018).

4.1.1 Target CPM precipitation

We aim to emulate the daily mean precipitation output over England and Wales from the Met Office UK CPM. This dynamical model has a grid spacing of 2.2km covering the UK. To provide boundary conditions for the UK CPM, Met Office GCM simulations with 60km grid spacing are first dynamically downscaled using a 12km RCM (Kendon et al. 2021). The domain for the 12km RCM is the EURO-CORDEX grid (Jacob et al. 2014) which covers Europe and parts of the North Atlantic and North Africa (see <https://cordex.org/domains/cordex-region-euro-cordex/> for full definition). The boundary conditions for the UK CPM are then derived from the RCM simulations. The CPM has a skilful representation of convective processes and captures small-scale rainfall systems that are not resolved in the driving GCM (Kendon et al. 2012; Kendon et al. 2014; Kendon et al. 2020).

We use data from 12 ensemble members. Each member uses a GCM/RCM pair with unique parameter settings, but an identical CPM. The simulations follow the Representative Concentration Pathway 8.5 (RCP8.5) climate forcing scenario. We use data from three time periods provided in the initial 2021 release of UKCP Local, which we refer to as “Historic” for 1981–2000, “Present” for 2021–2040 and “Future” for 2061–2080. This gives a total of 720 years of

data, which allows development of an emulator that can learn to represent extreme events, and also allows evaluation on such cases.

The simulations use a 360-day year, consisting of twelve 30-day months. Simulations begin on 1st December of a given year, so we take each numbered year to run between 1st December to 30th November (e.g. 1981 means 1st December 1980 to 30th November 1981).

We use daily-mean data from the CPM. For our target high-resolution precipitation, we coarsen the CPM output to 8.8km grid spacing using conservative interpolation and extract the England and Wales domain. The scale of resolved features in dynamical climate models is generally several times the grid box spacing (Klaver et al. 2020), so this coarsening captures the better resolved scales. This coarsening also allows a good trade off between resolution and domain size and compute requirements. The emulator can run well on commodity hardware such as a 10GB NVIDIA GeForce RTX 2080 Ti graphics processing unit. This precipitation resolution in space and time is superior to that recently used for state-of-the-art UK flood risk modelling (Bates et al. 2023), so it is at a useful scale for climate impacts assessment, while the domain is large enough to visualise features such as fronts and mesoscale convective organisation. There are no clear barriers to increasing the spatial resolution and domain size other than access to computing resources.

4.1.2 Coarse predictors

We use coarse-resolution predictors across the whole England and Wales domain. Note these are different to the inputs used by the CPM, whereby GCM data is supplied at the boundary of the intermediate 12km RCM and for prescribing sea surface temperatures. We describe our method as an “emulator” in the sense that it is developed to predict high-resolution precipitation corresponding to a given GCM simulation that has the same properties as precipitation from the CPM. This approach has the benefit of using the physics embedded in the GCM to predict reasonably realistic weather states at coarse-resolution.

Ideally we could learn a mapping directly from GCM variables, with 60km grid spacing, to high resolution CPM precipitation. However, synoptic-scale features in a CPM and its driving GCM simulation are not always well-aligned, due to internal variability in the CPM and intermediate RCM (also discussed by Doury et al. (2023)). For example, the GCM may simulate precipitation in the west of the UK whilst it is in the east in the CPM on the same day due to a difference in the exact positioning of a weather front. This means that a mapping directly between GCM and CPM variables is very noisy. Instead, we follow the same approach as Doury et al. (2023) and train using data from the CPM that has been coarsened to the GCM resolution using conservative interpolation (referred to as “cCPM”). This ensures that during training, the weather features in the coarse- and high-resolution data are aligned. Once trained, the emulator can use either coarsened CPM variables or GCM variables as inputs. This approach to training requires there to be sufficient statistical similarity between coarsened CPM and GCM predictor variables.

We have selected predictors of precipitation based on those that have been found useful in previous statistical downscaling work (e.g. Gutiérrez et al. 2019) and based on the understanding of the physical drivers of precipitation (Chan et al. 2018). Since we train the emulator using coarsened CPM variables as input with the aim to apply it using GCM variables, it is important to select variables that are represented to a similar degree of realism in the CPM and GCM. It is also important to select variables where the direction of causal influence is primarily from the variables to the high-resolution precipitation. For these reasons, we avoid using the coarse-resolution precipitation or variables in the boundary layer (below ~ 850 hPa) as predictors. We tested several choices of coarse-resolution predictor variables during the emulator development. In our final design, we use pressure at mean sea level and three variables on levels in the free troposphere: specific humidity, temperature and vorticity of the horizontal wind components. For these multi-level variables, we use a range of altitudes (250, 500, 700 and 850 hPa), similar to previous works (e.g. Gutiérrez et al. 2019; Doury et al. 2023). We use the vorticity rather than the full wind field because vorticity has been found to be a good predictor of convection (Chan et al. 2018) and the divergent component of the horizontal wind and the vertical wind

component may be more strongly affected by feedbacks from convection. Vorticity is calculated from eastward and northward wind components on the coarse 60km grid. Note the inputs for the emulator are different to the inputs used by the CPM, whereby GCM data is supplied at the boundary of the intermediate 12km RCM and for prescribing sea surface temperatures. The full set of coarse input variables to the emulator are:

- pressure at mean sea level
- specific humidity at 850, 700, 500 and 250 hPa
- vorticity at 850, 700, 500 and 250 hPa
- temperature at 850, 700, 500 and 250 hPa

4.2 ML Models

4.2.1 Diffusion model-based emulator

Figure 1 shows an overview of the emulator’s inputs, outputs and domain. Inputs and outputs are daily means from the same day and cover the same spatial domain. The inputs are the coarse variables described above. The emulator is stochastic and can generate an arbitrary number of samples of high-resolution precipitation for given coarse-resolution inputs. This means the emulator can learn to represent the inherent stochastic component of the downscaling task. Ideally, the distribution of these samples matches the distribution of high-resolution precipitation that the CPM would produce over many runs using the same driving GCM data, though we cannot directly test this.

The emulator is a diffusion model based on the work of Song et al. (2021). The training process of a diffusion model proceeds by first adding noise in many steps to target samples (precipitation fields in our case) so that they resemble pure noise after the final step. Then a neural network is trained to assist computing of a process which reverses this noising (again over many steps) and thus can be used to turn pure noise into samples from the target distribution (see [Supplementary Materials S1](#) for a fuller description). For our emulator we use Song et al. (2021)’s sub-Variance-Preserving (“sub-VP”) formulation of the stochastic differential equation (SDE) that defines the noise-adding process in their framework. We use their NCSN++ configuration (an improved version of their original Noise Conditional Score Network) as the backbone neural network. We have adapted it to use conditioning information by creating an input to the network based on the coarsened variables and the target field that is to be denoised. We do this by regridding the coarsened variables to the target grid using a nearest neighbour approach and then stacking these upsampled fields with the target field. We added a final single-channel convolutional layer so that the output (the reduced noised version of our noisy target field in the inputs) matches the size of our target. This final network has ~63M parameters. We train for 20 epochs on the training dataset, after which further training did not show improvements to the loss computed on the validation set nor to our evaluation metrics computed on samples based on the validation set. We use the Euler-Maruyama method to solve the reverse SDE for generating samples with the fitted network. On commodity hardware, a single 10GB NVIDIA GeForce RTX 2080 Ti GPU, training took approximately 41 hours.

We generated 6 samples for each day. Each set of samples for a single ensemble member’s portion of the test dataset (9 years) took approximately 5 hours to generate on the same hardware (so approximately 360 hours for 6 sample sets for all 108 years from 12 ensemble members, though this can be trivially parallelized across multiple GPUs if available). By comparison, a 20 year simulation of the CPM requires 6 months using several hundred CPUs. The implementation (including full configuration) is available on Github: <https://github.com/henryaddison/mlde>, which is a fork of https://github.com/yang-song/score_sde_pytorch (Song et al. 2021). The the configuration of our final diffusion emulator can be found in `ukcp_local_pr_12em_cncsnpp_continuous.py`.

4.2.2 U-Net comparison method

We compare results against a deterministic U-Net (Ronneberger et al. 2015). The U-Net architecture has been shown to perform well in similar climate downscaling settings (e.g. Doury et al. 2023; Meer et al. 2023). We use a U-Net based on the original architecture by Ronneberger et al. (2015) with adjustments to match the resolution and number of input and output channels of our dataset (64x64 resolution, 13 input channels, 1 output channel). As with the diffusion emulator, the coarse input variables are regridded to the target grid using nearest neighbour approach so the the input and output resolutions are the same. The network has ~ 17 M parameters. We train over 100 epochs using a mean squared error loss function (this is a different loss function to that used with the diffusion model so number of epochs are not expected to be the same). Whilst performance may be improved by using an alternative loss function (e.g. Doury et al. 2024), the advantages and disadvantages of particular loss functions are not yet fully clear, and an approach has not yet been found that results in a U-Net producing predictions with realistic small-scale structure, one of our primary aims. So we have chosen to focus on mean squared error loss here.

We also compare emulator predictions with a coarsened version of the CPM precipitation (“cCPM Bilinear”). We coarsen it to 60km grid spacing with conservative interpolation, then project it back to 8.8km resolution with bilinear interpolation. Comparison between this and emulator samples indicates the effect of the emulator adding detail at scales finer than the grid spacing of the predictor variables. Note we do not necessarily expect the emulator outputs to share all the large-scale features as cCPM-Bilinear in individual predictions, as these are not necessarily deterministically predictable from the input variables.

4.3 Training

4.3.1 Dataset splits

The dataset is divided into training, validation and test subsets. The training dataset was used to fit the model parameter values (including for transforming the variables, described below). Results for different emulator designs (e.g. choices of predictor variables and transformations) were checked on the validation dataset and used to select the final version. All results shown in this manuscript are based on the test dataset, giving an unbiased estimate of the emulator’s quality. The data can be found on Zenodo (Addison et al. 2024): <https://doi.org/10.5281/zenodo.11504859>.

For each 20 year time period, the training dataset includes 14 years in total (70%) and the validation and test datasets include 3 years each (15%). This is done by selecting whole seasons (Spring, Summer, Autumn and Winter) at random, with an equal number of each season in each subset. For each selected season we take data from all 12 CPM ensemble members, so that each subset has equal proportions across the ensemble members. For example, the test dataset is formed of three randomly chosen springs, summers, autumns and winters from each time period. Selecting data by season means we have minimal data leakage between the training, validation and test datasets due to auto-correlation between days, but also means the data in each subset cover a wide range of years and sample a representative set of climatic conditions, following Schultz et al. (2021).

4.3.2 Variable transformations

We apply several transformations of the data to improve the emulator’s performance. To produce target data for training the emulator’s neural network, we first take the square root of the precipitation to produce a less skewed distribution than the raw precipitation, which has many zero values and a long tail, to improve emulator performance. (An alternative approach is a log-based transformation (e.g. Harris et al. 2022), but this led to unrealistic samples being output by our diffusion model.) Then we linearly map the square rooted values so that those in the training dataset lie in the interval $[-1, 1]$. This is inverted upon sampling, and any negative value increased to 0 before squaring (this clipping affects about 15% of values, but in practice all are

very small: if they were positive values, they would all correspond to precipitation amounts less than 0.15mm/day, with 90% of cases under 0.003mm/day).

Input variables are standardised using their mean and standard deviation across the whole domain in the coarsened CPM training subset.

4.3.3 Bias correction of GCM inputs

When using predictor variables from the GCM, it was found to be beneficial to bias-correct their means and standard deviations to those of the coarsened CPM variables, to account for systematic differences between the GCM and CPM variables at coarse resolution. This was done for each coarse grid box separately based on the training dataset and applied before the other transformations above. The bias-corrected value of variable x at grid box g is

$$\left(\frac{x_g - \bar{x}_g^{GCM}}{s_g^{GCM}} \right) s_g^{CPM} + \bar{x}_g^{CPM} \quad (1)$$

where \bar{x}_g^{GCM} and s_g^{GCM} are the mean and standard deviation of the values of x taken from GCM at grid box g from the training split, and \bar{x}_g^{CPM} and s_g^{CPM} are the equivalent for CPM-sourced values of the variable.

4.4 Radially Averaged Power Spectral Density

We use RAPSD to compare the complexity of structures produced by different approaches (or the variability over different spatial scales) (Harris et al. 2001; Sinclair and Pegram 2005). To compute the power spectrum of a precipitation field, we compute the 2D Fourier transform of the field and convert to power by multiplying by complex conjugate. We then radially average over nested annuli centred on the origin in the 2D spatial frequency space to create a 1D vector of power at different frequency bands. Finally to compare difference approaches, we compute mean for each frequency band over all samples.

4.5 Bootstrapping domain mean change confidence intervals

We use bootstrapping (Efron 1982) to estimate the variance of the seasonal domain mean change in precipitation from Historic to Future time periods for our emulator. In particular, to estimate 95% confidence intervals of the values. For a given season and time period, we sample with replacement from the set of 36 seasonal domain means across the ensemble members and time period (12 ensemble member by 3 years) to produce paired estimates of both the CPM domain mean and emulator domain mean. By repeating this resampling 100,000 times for both time periods we estimate 0.025 and 0.975 quantiles for the difference in CPU emulator of the change from Historic to Future time periods.

References

- Kendon, E. J., N. M. Roberts, C. A. Senior and M. J. Roberts (2012). “Realism of Rainfall in a Very High-Resolution Regional Climate Model”. In: *Journal of Climate* 25.17, pp. 5791–5806. ISSN: 0894-8755. DOI: [10.1175/JCLI-D-11-00562.1](https://doi.org/10.1175/JCLI-D-11-00562.1).
- Kendon, E. J., C. Short, J. Pope, S. Chan, J. Wilkinson, S. Tucker, P. Bett and G. Harris (2021). “Update to UKCP Local (2.2km) projections”. In.
- Sobolowski, S., S. Somot, J. Fernandez, G. Evin, D. Maraun, S. Kotlarski, M. Jury, R. E. Benestad, C. Teichmann, O. B. Christensen, B. Katharina, E. Buonomo, E. Katragkou, C. Steger, S. Sørland, G. Nikulin, C. McSweeney, A. Dobler, T. Palmer, R. Wilke, J. Boé, L. Brunner, A. Ribes, S. Qasmi, P. Nabat, F. Sevault, T. Oudar and S. Brands (Feb. 2023). *EURO-CORDEX CMIP6 GCM Selection & Ensemble Design: Best Practices and Recommendations*. DOI: [10.5281/zenodo.7673400](https://doi.org/10.5281/zenodo.7673400).

- Maher, N., S. Milinski and R. Ludwig (2021). “Large ensemble climate model simulations: introduction, overview, and future prospects for utilising multiple types of large ensemble”. In: *Earth System Dynamics* 12.2, pp. 401–418. ISSN: 2190-4987.
- Leach, N. J., P. A. G. Watson, S. N. Sparrow, D. C. H. Wallom and D. M. H. Sexton (2022). “Generating samples of extreme winters to support climate adaptation”. In: *Weather and Climate Extremes* 36, p. 100419. ISSN: 22120947. DOI: [10.1016/j.wace.2022.100419](https://doi.org/10.1016/j.wace.2022.100419).
- Eyring, V., S. Bony, G. A. Meehl, C. A. Senior, B. Stevens, R. J. Stouffer and K. E. Taylor (2016). “Overview of the Coupled Model Intercomparison Project Phase 6 (CMIP6) experimental design and organization”. In: *Geoscientific Model Development* 9.5. GMD, pp. 1937–1958. ISSN: 1991-9603. DOI: [10.5194/gmd-9-1937-2016](https://doi.org/10.5194/gmd-9-1937-2016).
- Sohl-Dickstein, J., E. Weiss, N. Maheswaranathan and S. Ganguli (2015). “Deep unsupervised learning using nonequilibrium thermodynamics”. In: *International conference on machine learning*. PMLR, pp. 2256–2265.
- Song, Y., J. Sohl-Dickstein, Diederik, A. Kumar, S. Ermon and B. Poole (2021). “Score-Based Generative Modeling through Stochastic Differential Equations”. In: *ICLR*. DOI: [arxiv:2011.13456](https://arxiv.org/abs/2011.13456).
- Bates, P. D., J. Savage, O. Wing, N. Quinn, C. Sampson, J. Neal and A. Smith (2023). “A climate-conditioned catastrophe risk model for UK flooding”. In: *Natural Hazards and Earth System Sciences* 23.2. NHESS, pp. 891–908. ISSN: 1684-9981. DOI: [10.5194/nhess-23-891-2023](https://doi.org/10.5194/nhess-23-891-2023).
- Kendon, E. J., E. M. Fischer and C. J. Short (2023). “Variability conceals emerging trend in 100yr projections of UK local hourly rainfall extremes”. In: *Nat Commun* 14.1, p. 1133. ISSN: 2041-1723 (Electronic) 2041-1723 (Linking). DOI: [10.1038/s41467-023-36499-9](https://doi.org/10.1038/s41467-023-36499-9).
- Schoof, J. T. (2013). “Statistical Downscaling in Climatology”. In: *Geography Compass* 7.4, pp. 249–265. ISSN: 1749-8198 1749-8198. DOI: [10.1111/gec3.12036](https://doi.org/10.1111/gec3.12036).
- Maraun, D. and M. Widmann (2018). *Statistical downscaling and bias correction for climate research*. Cambridge University Press. ISBN: 1108340644.
- Maraun, D., M. Widmann and J. M. Gutierrez (2019). “Statistical downscaling skill under present climate conditions: A synthesis of the VALUE perfect predictor experiment”. In: *International Journal of Climatology* 39.9, pp. 3692–3703. DOI: [10.1002/joc.5877](https://doi.org/10.1002/joc.5877).
- Widmann, M., J. Bedia, J. M. Gutierrez, T. Bosshard, E. Hertig, D. Maraun, M. J. Casado, P. Ramos, R. M. Cardoso, P. M. M. Soares, J. Ribalaygua, C. Page, A. M. Fischer, S. Herrera and R. Huth (2019). “Validation of spatial variability in downscaling results from the VALUE perfect predictor experiment”. In: *International Journal of Climatology* 39.9, pp. 3819–3845. DOI: [10.1002/joc.6024](https://doi.org/10.1002/joc.6024).
- Schaller, N., J. Sillmann, M. Muller, R. Haarsma, W. Hazeleger, T. J. Hegdahl, T. Kelder, G. van den Oord, A. Weerts and K. Whan (2020). “The role of spatial and temporal model resolution in a flood event storyline approach in western Norway”. In: *Weather and Climate Extremes* 29, p. 100259. DOI: [10.1016/j.wace.2020.100259](https://doi.org/10.1016/j.wace.2020.100259).
- Archer, L., S. Hatchard, L. Devitt, J. C. Neal, G. Coxon, P. D. Bates, E. J. Kendon and J. Savage (2024). “Future Change in Urban Flooding Using New Convection-Permitting Climate Projections”. In: *Water Resources Research* 60.1, e2023WR035533. DOI: <https://doi.org/10.1029/2023WR035533>.
- Maraun, D., T. G. Shepherd, M. Widmann, G. Zappa, D. Walton, J. M. Gutiérrez, S. Hagemann, I. Richter, P. M. M. Soares, A. Hall and L. O. Mearns (2017). “Towards process-informed bias correction of climate change simulations”. In: *Nature Climate Change* 7.11, pp. 764–773. ISSN: 1758-678X. DOI: [10.1038/nclimate3418](https://doi.org/10.1038/nclimate3418).
- Vosper, E., P. Watson, L. Harris, A. McRae, R. Santos-Rodriguez, L. Aitchison and D. Mitchell (2023). “Deep Learning for Downscaling Tropical Cyclone Rainfall to Hazard-Relevant Spatial Scales”. In: *Journal of Geophysical Research-Atmospheres* 128.10, e2022JD038163. DOI: [10.1029/2022JD038163](https://doi.org/10.1029/2022JD038163).
- Harris, L., A. T. T. McRae, M. Chantry, P. D. Dueben and T. N. Palmer (2022). “A Generative Deep Learning Approach to Stochastic Downscaling of Precipitation Forecasts”. In: *J Adv Model Earth Syst* 14.10, e2022MS003120. DOI: [10.1029/2022MS003120](https://doi.org/10.1029/2022MS003120).

- Leinonen, J., D. Nerini and A. Berne (2020). “Stochastic Super-Resolution for Downscaling Time-Evolving Atmospheric Fields With a Generative Adversarial Network”. In: *IEEE Transactions on Geoscience and Remote Sensing*, pp. 1–13.
- Vandal, T., E. Kodra and A. R. Ganguly (2018). “Intercomparison of machine learning methods for statistical downscaling: the case of daily and extreme precipitation”. In: *Theoretical and Applied Climatology* 137.1-2, pp. 557–570. DOI: [10.1007/s00704-018-2613-3](https://doi.org/10.1007/s00704-018-2613-3).
- Sha, Y. K., D. J. Gagne, G. West and R. Stull (2020). “Deep-Learning-Based Gridded Downscaling of Surface Meteorological Variables in Complex Terrain. Part II: Daily Precipitation”. In: *Journal of Applied Meteorology and Climatology* 59.12, pp. 2075–2092. DOI: [10.1175/Jamc-D-20-0058.1](https://doi.org/10.1175/Jamc-D-20-0058.1).
- Wang, F., D. Tian and M. Carroll (2023). “Customized deep learning for precipitation bias correction and downscaling”. In: *Geoscientific Model Development* 16.2. GMD, pp. 535–556. ISSN: 1991-9603. DOI: [10.5194/gmd-16-535-2023](https://doi.org/10.5194/gmd-16-535-2023).
- Doury, A., S. Somot and S. Gadat (2024). “On the suitability of a Convolutional Neural Network based RCM-Emulator for fine spatio-temporal precipitation”. In: *Climate Dynamics*.
- Ravuri, S., K. Lenc, M. Willson, D. Kangin, R. Lam, P. Mirowski, M. Fitzsimons, M. Athanassiadou, S. Kashem, S. Madge, R. Prudden, A. Mandhane, A. Clark, A. Brock, K. Simonyan, R. Hadsell, N. Robinson, E. Clancy, A. Arribas and S. Mohamed (2021). “Skilful precipitation nowcasting using deep generative models of radar”. In: *Nature* 597.7878, pp. 672–677. DOI: [10.1038/s41586-021-03854-z](https://doi.org/10.1038/s41586-021-03854-z).
- Hess, P., M. Druke, S. Petri, F. M. Strnad and N. Boers (2022). “Physically constrained generative adversarial networks for improving precipitation fields from Earth system models”. In: *Nature Machine Intelligence* 4.10, pp. 828–839. DOI: [10.1038/s42256-022-00540-1](https://doi.org/10.1038/s42256-022-00540-1).
- Addison, H., E. J. Kendon, S. Ravuri, L. Aitchison and P. Watson (2022). “Machine learning emulation of a local-scale UK climate model”. In: *NeurIPS 2022 Workshop on Tackling Climate Change with Machine Learning*.
- Mardani, M., N. Brenowitz, Y. Cohen, J. Pathak, C.-Y. Chen, C.-C. Liu, A. Vahdat, K. Kashinath, J. Kautz and M. Pritchard (2023). “Residual Diffusion Modeling for Km-scale Atmospheric Downscaling”. In: *arXiv preprint arXiv:2309.15214*.
- Gutiérrez, J. M., D. Maraun, M. Widmann, R. Huth, E. Hertig, R. Benestad, O. Roessler, J. Wibig, R. Wilcke, S. Kotlarski, D. San Martín, S. Herrera, J. Bedia, A. Casanueva, R. Manzananas, M. Iturbide, M. Vrac, M. Dubrovsky, J. Ribalaygua, J. Pórtoles, O. Räty, J. Räisänen, B. Hingray, D. Raynaud, M. J. Casado, P. Ramos, T. Zerenner, M. Turco, T. Bosshard, P. Štěpánek, J. Bartholy, R. Pongracz, D. E. Keller, A. M. Fischer, R. M. Cardoso, P. M. M. Soares, B. Czernecki and C. Pagé (2019). “An intercomparison of a large ensemble of statistical downscaling methods over Europe: Results from the VALUE perfect predictor cross-validation experiment”. In: *International Journal of Climatology* 39.9, pp. 3750–3785. DOI: [10.1002/joc.5462](https://doi.org/10.1002/joc.5462).
- Walton, D. B., F. P. Sun, A. Hall and S. Capps (2015). “A Hybrid Dynamical-Statistical Downscaling Technique. Part I: Development and Validation of the Technique”. In: *Journal of Climate* 28.12, pp. 4597–4617. DOI: [10.1175/Jcli-D-14-00196.1](https://doi.org/10.1175/Jcli-D-14-00196.1).
- Boé, J., A. Mass and J. Deman (2022). “A simple hybrid statistical–dynamical downscaling method for emulating regional climate models over Western Europe. Evaluation, application, and role of added value?” In: *Climate Dynamics* 61.1-2, pp. 271–294. ISSN: 0930-7575 1432-0894. DOI: [10.1007/s00382-022-06552-2](https://doi.org/10.1007/s00382-022-06552-2).
- Doury, A., S. Somot, S. Gadat, A. Ribes and L. Corre (2023). “Regional climate model emulator based on deep learning: concept and first evaluation of a novel hybrid downscaling approach”. In: *Climate Dynamics* 60.5-6, pp. 1751–1779. ISSN: 0930-7575 1432-0894. DOI: [10.1007/s00382-022-06343-9](https://doi.org/10.1007/s00382-022-06343-9).
- Kendon, E. J., N. M. Roberts, H. J. Fowler, M. J. Roberts, S. C. Chan and C. A. Senior (2014). “Heavier summer downpours with climate change revealed by weather forecast resolution model”. In: *Nature Climate Change* 4.7, pp. 570–576. ISSN: 1758-678X 1758-6798. DOI: [10.1038/nclimate2258](https://doi.org/10.1038/nclimate2258).

- Watson, P. A. G. (2022). “Machine learning applications for weather and climate need greater focus on extremes”. In: *Environmental Research Letters* 17.11, p. 111004. ISSN: 1748-9326. DOI: [10.1088/1748-9326/ac9d4e](https://doi.org/10.1088/1748-9326/ac9d4e).
- Watson, P. (2023). “Machine learning applications for weather and climate predictions need greater focus on extremes: 2023 update”. In: *NeurIPS 2023 Workshop on Tackling Climate Change with Machine Learning*.
- Leutbecher, M. and T. N. Palmer (2008). “Ensemble forecasting”. In: *Journal of Computational Physics* 227.7, pp. 3515–3539. DOI: [10.1016/j.jcp.2007.02.014](https://doi.org/10.1016/j.jcp.2007.02.014).
- Haynes, K., R. Lagerquist, M. McGraw, K. Musgrave and I. Ebert-Uphoff (2023). “Creating and Evaluating Uncertainty Estimates with Neural Networks for Environmental-Science Applications”. In: *Artificial Intelligence for the Earth Systems* 2.2, p. 220061. ISSN: 2769-7525. DOI: [10.1175/aies-d-22-0061.1](https://doi.org/10.1175/aies-d-22-0061.1).
- Kendon, E. J., H. Addison, A. Doury, B. B. Booth, S. Somot, P. A. G. Watson, L. Aitchison, E. Coppola, J. M. Gutierrez and J. Murphy (2024). “Potential for machine learning emulators to augment regional climate simulations in provision of local climate change information”. In: *Bulletin of the American Meteorological Society*. In preparation.
- Kendon, E. J., N. Ban, N. M. Roberts, H. J. Fowler, M. J. Roberts, S. C. Chan, J. P. Evans, G. Fosser and J. M. Wilkinson (2017). “Do Convection-Permitting Regional Climate Models Improve Projections of Future Precipitation Change?” In: *Bulletin of the American Meteorological Society* 98.1, pp. 79–93. DOI: [10.1175/bams-d-15-0004.1](https://doi.org/10.1175/bams-d-15-0004.1).
- Chan, S. C., E. J. Kendon, S. Berthou, G. Fosser, E. Lewis and H. J. Fowler (2020). “Europe-wide precipitation projections at convection permitting scale with the Unified Model”. In: *Clim Dyn* 55.3, pp. 409–428. ISSN: 0930-7575 (Print) 1432-0894 (Electronic) 0930-7575 (Linking). DOI: [10.1007/s00382-020-05192-8](https://doi.org/10.1007/s00382-020-05192-8).
- Kendon, E. J., R. A. Stratton, S. Tucker, J. H. Marsham, S. Berthou, D. P. Rowell and C. A. Senior (2019). “Enhanced future changes in wet and dry extremes over Africa at convection-permitting scale”. In: *Nat Commun* 10.1, p. 1794. ISSN: 2041-1723 (Electronic) 2041-1723 (Linking). DOI: [10.1038/s41467-019-09776-9](https://doi.org/10.1038/s41467-019-09776-9).
- Blattmann, A., R. Rombach, H. Ling, T. Dockhorn, S. W. Kim, S. Fidler and K. Kreis (2023). “Align your latents: High-resolution video synthesis with latent diffusion models”. In: *Proceedings of the IEEE/CVF Conference on Computer Vision and Pattern Recognition*, pp. 22563–22575.
- Bar-Tal, O., H. Chefer, O. Tov, C. Herrmann, R. Paiss, S. Zada, A. Ephrat, J. Hur, Y. Li and T. Michaeli (2024). “Lumiere: A space-time diffusion model for video generation”. In: *arXiv preprint arXiv:2401.12945*.
- Harvey, W., S. Naderiparizi, V. Masrani, C. Weilbach and F. Wood (2022). “Flexible diffusion modeling of long videos”. In: vol. 35, pp. 27953–27965.
- Murphy, J., G. Harris, D. Sexton, E. Kendon, P. Bett, R. Clark, K. Eagle, G. Fosser, F. Fung and J. Lowe (2018). “UKCP18 land projections: science report”. In.
- Jacob, D., J. Petersen, B. Eggert, A. Alias, O. B. Christensen, L. M. Bouwer, A. Braun, A. Colette, M. Déqué, G. Georgievski, E. Georgopoulou, A. Gobiet, L. Menut, G. Nikulin, A. Haensler, N. Hempelmann, C. Jones, K. Keuler, S. Kovats, N. Kröner, S. Kotlarski, A. Kriegsmann, E. Martin, E. van Meijgaard, C. Moseley, S. Pfeifer, S. Preuschmann, C. Radermacher, K. Radtke, D. Rechid, M. Rounsevell, P. Samuelsson, S. Somot, J. F. Soussana, C. Teichmann, R. Valentini, R. Vautard, B. Weber and P. Yiou (2014). “EURO-CORDEX: new high-resolution climate change projections for European impact research”. In: *Regional Environmental Change* 14.2, pp. 563–578. ISSN: 1436-3798. DOI: [10.1007/s10113-013-0499-2](https://doi.org/10.1007/s10113-013-0499-2).
- Kendon, E. J., N. M. Roberts, G. Fosser, G. M. Martin, A. P. Lock, J. M. Murphy, C. A. Senior and S. O. Tucker (2020). “Greater Future U.K. Winter Precipitation Increase in New Convection-Permitting Scenarios”. In: *Journal of Climate* 33.17, pp. 7303–7318. ISSN: 0894-8755 1520-0442. DOI: [10.1175/jcli-d-20-0089.1](https://doi.org/10.1175/jcli-d-20-0089.1).
- Klaver, R., R. Haarsma, P. L. Vidale and W. Hazeleger (2020). “Effective resolution in high resolution global atmospheric models for climate studies”. In: *Atmospheric Science Letters* 21.4, e952. ISSN: 1530-261X. DOI: [10.1002/as1.952](https://doi.org/10.1002/as1.952).

- Chan, S. C., E. J. Kendon, N. Roberts, S. Blenkinsop and H. J. Fowler (2018). “Large-Scale Predictors for Extreme Hourly Precipitation Events in Convection-Permitting Climate Simulations”. In: *Journal of Climate* 31.6, pp. 2115–2131. ISSN: 0894-8755. DOI: [10.1175/Jcli-D-17-0404.1](https://doi.org/10.1175/Jcli-D-17-0404.1).
- Ronneberger, O., P. Fischer and T. Brox (2015). “U-Net: Convolutional Networks for Biomedical Image Segmentation”. In: *Medical Image Computing and Computer-Assisted Intervention, Pt Iii* 9351, pp. 234–241. ISSN: 0302-9743. DOI: [10.1007/978-3-319-24574-4_28](https://doi.org/10.1007/978-3-319-24574-4_28).
- Meer, M. van der, S. de Roda Husman and S. Lhermitte (2023). “Deep Learning Regional Climate Model Emulators: A Comparison of Two Downscaling Training Frameworks”. In: *Journal of Advances in Modeling Earth Systems* 15.6, e2022MS003593. DOI: [10.1029/2022ms003593](https://doi.org/10.1029/2022ms003593).
- Addison, H., E. Kendon, S. Ravuri, L. Aitchison and P. A. Watson (June 2024). *Met Office UKCP Local CPM precipitation ML emulator dataset*. Version 1.0.0. Zenodo. DOI: [10.5281/zenodo.11504859](https://doi.org/10.5281/zenodo.11504859).
- Schultz, M. G., C. Betancourt, B. Gong, F. Kleinert, M. Langguth, L. H. Leufen, A. Mozaffari and S. Stadtler (2021). “Can deep learning beat numerical weather prediction?” In: *Philosophical Transactions of the Royal Society A: Mathematical, Physical and Engineering Sciences* 379.2194, p. 20200097. ISSN: 1364-503X. DOI: [10.1098/rsta.2020.0097](https://doi.org/10.1098/rsta.2020.0097).
- Harris, D., E. Foufoula-Georgiou, K. K. Droegemeier and J. J. Levit (2001). “Multiscale statistical properties of a high-resolution precipitation forecast”. In: *Journal of Hydrometeorology* 2.4, pp. 406–418. DOI: [10.1175/1525-7541\(2001\)002<0406:Msपोह>2.0.Co;2](https://doi.org/10.1175/1525-7541(2001)002<0406:Msपोह>2.0.Co;2).
- Sinclair, S. and G. G. S. Pegram (2005). “Empirical Mode Decomposition in 2-D space and time: a tool for space-time rainfall analysis and nowcasting”. In: *Hydrology and Earth System Sciences* 9.3, pp. 127–137. DOI: [DOI10.5194/hess-9-127-2005](https://doi.org/10.5194/hess-9-127-2005).
- Efron, B. (1982). *The jackknife, the bootstrap and other resampling plans*. SIAM. ISBN: 0898711797.
- Song, Y. and S. Ermon (n.d.). “Generative modeling by estimating gradients of the data distribution”. In: *Advances in Neural Information Processing Systems*. Vol. 32.
- Ho, J., A. Jain and P. Abbeel (2020). “Denoising diffusion probabilistic models”. In: *Advances in Neural Information Processing Systems*. Vol. 33, pp. 6840–6851.

Acknowledgments

Funding: HA was supported by the UKRI Centre for Doctoral Training in Interactive Artificial Intelligence under Grant EP/S022937/1. EJK was supported by the Met Office Hadley Centre Climate Programme funded by DSIT under Grant GA01101. PAGW was supported by a Natural Environment Research Council Independent Research Fellowship (grant no. NE/S014713/1). We would like to thank Dr Stewart for compute resources used in the project, along with Bristol’s ACRC for maintaining the cluster.

Author contributions:

- Conceptualization: HA, EJK, LA, PAGW
- Data curation: HA
- Formal Analysis: HA, LA, PAGW
- Methodology: HA, EJK, SR, LA, PAGW
- Investigation: HA, LA, PAGW
- Visualization: HA, LA, PAGW
- Resources: LA, PAGW
- Software: HA
- Supervision: EJK, SR, LA, PAGW
- Writing—original draft: HA, PAGW

- Writing—review & editing: HA, EJK, SR, LA, PAGW

Competing interests: The authors declare that they have no competing interests.

Data and materials availability: The data for training and evaluating the models is be available on Zenodo (Addison et al. 2024). Trained model weights and samples from ML models are available on request. The code will be available on GitHub. For processing the data: <https://github.com/henryaddison/mlde-data>. For training and sampling from the ML models: <https://github.com/henryaddison/mlde> and for evaluating the models: <https://github.com/henryaddison/mlde-notebooks>.

Supplementary Materials

S1 Diffusion models

Probabilistic models assume that observed data, such as high-resolution precipitation over the UK, is drawn from an unknown distribution $p^*(\mathbf{x})$. A conditional model such as our high-resolution precipitation emulator conditioned on coarse inputs $p^*(\mathbf{x}|\mathbf{y})$ can also be considered but for simplicity we will stick with the unconditional version.

Song et al. (2021) combine earlier approaches (Song and Ermon n.d.; Ho et al. 2020) into a single framework called Score-Based Generative Models with Stochastic Differential Equations (SDE). The idea is to imagine a diffusion process $\{\mathbf{x}(t)_{t=0}^T\}$ modelled by an SDE:

$$d\mathbf{x} = \mathbf{f}(\mathbf{x}, t)dt + g(t)d\mathbf{w} \quad (\text{S2})$$

When run forward, a sample, $\mathbf{x}(0)$, from the data distribution, p_0 , is gradually perturbed over time into a sample from a final noise distribution, p_T . The final distribution is chosen as something tractable for sampling, usually a Gaussian.

More interesting for us is running the reverse diffusion process:

$$d\mathbf{x} = [\mathbf{f}(\mathbf{x}, t) - g(t)^2 \nabla_{\mathbf{x}} \log p_t(x)]dt + g(t)d\bar{\mathbf{w}} \quad (\text{S3})$$

By solving this, samples from p_T (which are easy to produce by design) can be converted into samples from the original data distribution. This requires two steps: calculating the score, $\nabla_{\mathbf{x}} \log p_t(x)$, and then applying numerical approaches to solve Equation S3.

The score is estimated as a neural net $s_\theta(\mathbf{x}, t)$ where θ are determined by minimizing:

$$\mathbb{E}_t \{ \lambda(t) \mathbb{E}_{\mathbf{x}(0)} \mathbb{E}_{\mathbf{x}(0)|\mathbf{x}(t)} [\|s_\theta(\mathbf{x}(t), t) - \nabla_{\mathbf{x}(t)} \log p_{0t}(\mathbf{x}(t)|\mathbf{x}(0))\|_2^2] \} \quad (\text{S4})$$

where λ is a positive weighting function that is chosen along with \mathbf{f} and \mathbf{g} .

Song et al. (2021) summarize three approaches for solving the reverse SDE. General-purpose numerical methods can be used to find approximate solutions to the SDE. Predictor-Corrector sampling takes this a step further by using making use of estimated score at each timestep to apply a correction to the sample estimated at that timestep by the general purpose solver. Alternatively the problem can be reformulated as a deterministic process without affecting the trajectory probabilities and in turn solved using an ODE solver.

Season	CPM (%)	Diffusion-cCPM (%)	Difference (95% CI) (% of CPM change)	Difference (95% CI) (% of historic CPM)
DJF	23	18	-21 (-33 to -9)	-5 (-7.7 to -2.0)
MAM	6	4	-31 (-78 to +15)	-2 (-4.8 to +1.0)
JJA	-40	-39	2 (-10 to +7)	1 (-2.9 to +3.9)
SON	-4	-6	-59 (-8 to +129)	-2 (+0.3 to -5.1)

Table S3: Change in seasonal domain mean for Diffusion-cCPM. Shows changes in the domain mean from Historic to Future periods for each season. The second and third columns contain the relative changes for the CPM and Diffusion-cCPM respectively (relative to CPM historic seasonal domain mean in both cases). The fourth column contains the difference between the change in the CPM and Diffusion-cCPM, relative to the change in CPM. The values in brackets in these columns are the bootstrapped 95% confidence intervals of the difference. The fifth column is the same as the third but relative to the historic CPM seasonal domain mean.